39th AIAA/ASME/SAE/ASEE Joint Propulsion Conference and Exhibit
20-23 July 2003, Huntsville, Alabama

FUNCTION OF A HOLLOW ANODE FOR AN ANODE LAYER TYPE HALL THRUSTER

Shinsuke YASUI*, Ken KUMAKURA**, Naoji YAMAMOTO*,Kimiya KOMURASAKI**, and Yoshihiro ARAKAWA*
University of Tokyo, Tokyo 113-8656, JAPAN
* Department of Aeronautics and Astronautics
** Department of Advanced Energy
Email: yasui@al.t.u-tokyo.ac.jp

ABSTRACT

The amplitude of discharge current oscillation has been measured for various hollow anode widths and axial positions using a 1kW class anode layer type Hall thruster. As a result, there was plasma density threshold for stable discharge. Structure of electrical sheath inside a hollow anode was numerically analyzed using fully kinetic 2D3V Particle-in-Cell (PIC) and Direct Simulation Monte Carlo (DSMC) method. The computed sheath area was not so sensitive to the hollow width.

NOMENCLATURE

B: magnetic induction
D: anode hollow width
E: electric field strength
e: electronic charge
I: electric current
m: particle mass
n: number density
R: mean radius of the discharge channel
S: anode surface area
T: temperature
t: time
$\boldsymbol{v}$: velocity
V: voltage
x: position
Z: distance between anode tip and channel exit
ε_0: free space permeability
λ_D: Debye length
μ: magnetic permeability
τ : mean free time
ϕ : space potential
r, θ , z: cylindrical coordinate

SUBSCRIPTS

0 : anode exit
d : discharge
e : electron
i : ion
n : neutral
w : wall

INTRODUCTION

Discharge instability in anode layer type hall thrusters would be one of the serious problems to be overcome. A hollow anode is commonly used to stabilize the discharge for these thrusters as shown in Fig. 1.[1-3)]

However, the function of the hollow anode has not been clarified yet and optimization has not been done.

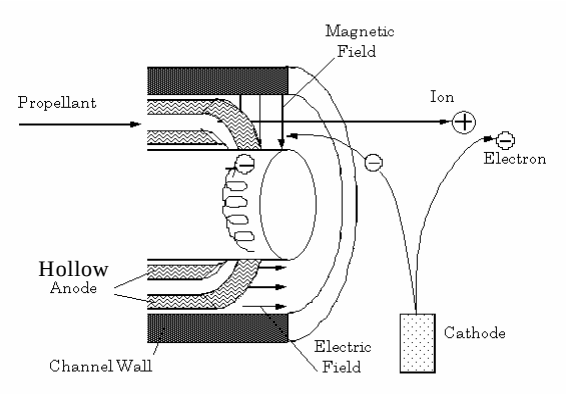

Fig. 1 Anode layer type Hall thruster.

In this research, the function of hollow anode is investigated experimentally and analytically. The goal of the study is to model the anode sheath, which has a great effect on the stable discharge of anode layer type hall thrusters, and find out a scaling law for the anode design.

In the experimental study, a 1kW class anode layer type hall thruster with a hollow anode has been designed and fabricated in university of Tokyo.[4)] (Fig. 2) Amplitude of discharge current oscillation has been measured for various hollow widths and axial positions.

As for the computational study, the structure of electrical sheath inside a hollow anode was numerically simulated using fully kinetic 2D3V Particle-in-Cell (PIC) and Direct Simulation Monte Carlo (DSMC) methodologies.[5-8)] Effects of geometric parameters on the sheath structure are investigated.

Fig. 2 1kW class anode-layer Hall Thruster.

EXPERIMENT

Thruster

The cross section of thruster is shown in Fig. 3. It has two guard rings made of stainless steel. They are kept at the cathode potential. The inner and outer diameters of a discharge chamber are 48mm and 62mm, respectively. A solenoidal coil is set at the center of the thruster to apply radial magnetic field in the discharge chamber. Magnetic induction is variable by changing coil current. As an electron source, a filament cathode (2% thoriated tungsten of f 0.27[mm] × 500[mm] × 3) was used to minimize discharge fluctuations originated from cathode operation instability.

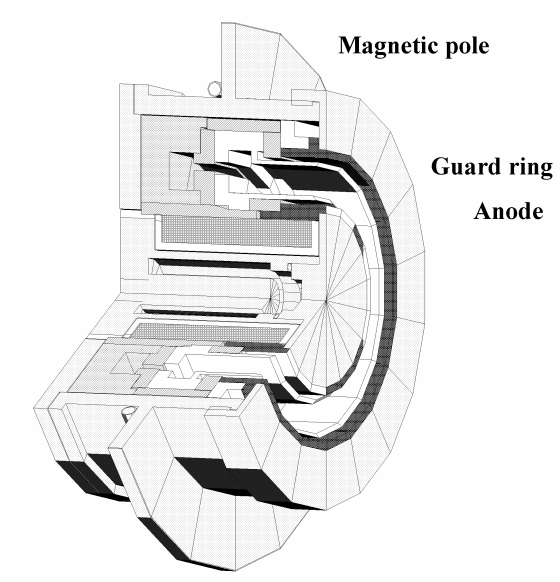

Fig. 3 The cross section of thruster.

Operating and geometric parameters

It has a hollow annular anode made of cupper. We define Z as the distance between the thruster exit and the tip of anode, and D as the width of propellant channel as indicated in Fig. 4. Z and D are varied (Z=1~4[mm], D=1~3[mm]) in this study. Xe is used as a propellant, and the mass flow rate is set at 1.0[A_{eq}]=1.37[mg/s]. Discharge voltage is set at 400[V]. Under such conditions, the amplitude of discharge current oscillation has been measured for various magnetic inductions.

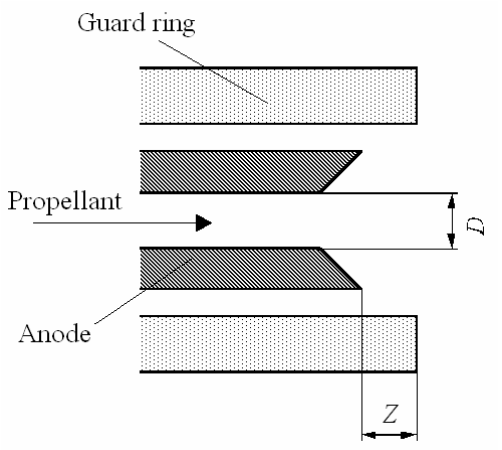

Fig. 4 Definitions of Z and D.

Discharge Stability

Figure 5 shows measured amplitude of discharge current oscillation and the discharge current. Here, the amplitude of discharge current oscillation is defined as,

$$\frac{I_d\_R.M.S}{\overline{I_d}} = \frac{1}{\overline{I_d}}\sqrt{\frac{\int_0^t (I_d - \overline{I_d})^2}{t}}, \quad (\overline{I_d} = \frac{\int_0^t I_d}{t}) \qquad (1)$$

Oscillation amplitude was sensitive to magnetic induction B. Although, the oscillation is small at B<0.014[T], the thrust efficiency is poor in this range of B because of large discharge current. Therefore, the desirable operation condition is limited in a quite narrow range of B.

Table 1 shows a map of the geometric parameters Z and D. In the map, discharge stability is denoted. The cases when oscillation amplitude is less than 0.1 are defined “stable.” Typically, stable discharge has not been realized for any B in the case of small Z and small D.

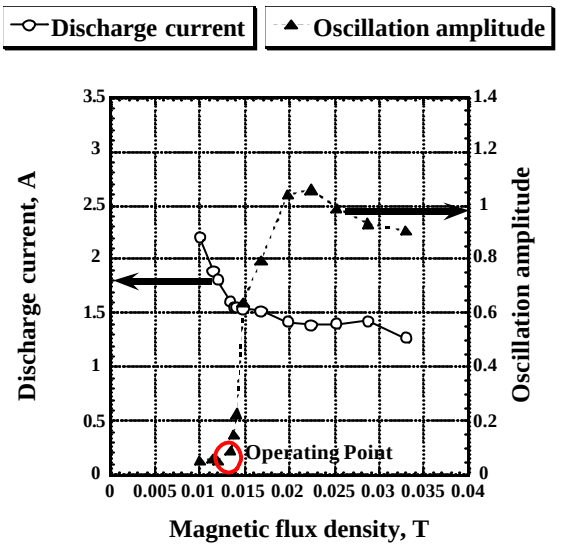

Fig. 5 Oscillation characteristics. *D*=3[mm], *Z*=1[mm].

Table 1 Discharge stability for various *D* and *Z*.

D[mm] \ Z[mm]	1	2	3	4
1	×	×	○	○
2	×	○	○	○
3	○	○	○	○

○: Stable ×: Unstable.

Measured oscillation amplitude is plotted in Fig. 6. There is a common trend that oscillation becomes unstable with the increase in *B* as seen in Fig. 5. However, the threshold of *B* varies depending on the geometric parameters *Z* and *D*.

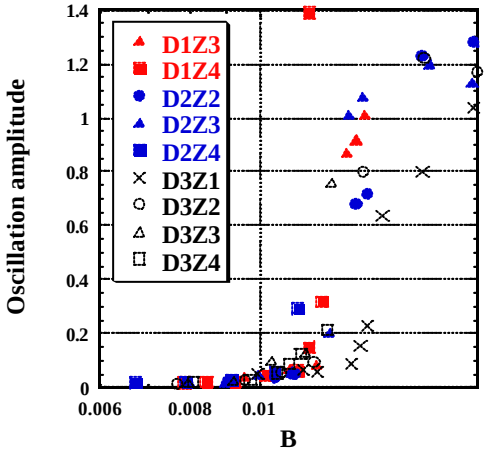

Fig. 6 Relation between oscillation amplitude and *B*. *Z*=1-4[mm], *D*=1-3[mm], *B*=0.006-0.02[T]

Unified parameter

Using a one dimensional electron diffusion model with a classical diffusion coefficient inside the discharge chamber, electron current can be expressed as

$$I_e = em_\perp n_e E\left(2pRD\right) = \frac{em_\parallel}{1+\left(m_\parallel B\right)^2} n_e E\left(2pRD\right)$$

$$\simeq \frac{e}{m_\parallel B^2} n_e E\left(2pRD\right) = \frac{m_e n_n < s\,v >}{B^2} n_e E\left(2pRD\right)$$

$$= \frac{\dot{m}_n}{m_n v_n} \frac{m_e < s\,v >}{B^2} n_e E \qquad (2)$$

Assuming uniform distributions of electric and magnetic fields, electron temperature, neutral and electron number densities and electron current density, Eq.(2) can be integrated in the z direction as

$$I_e B^2 Z = \frac{\dot{m}_n}{m_n v_n} m_e n_e < s\,v > V_d \qquad (3)$$

Then, electron density in the discharge chamber is expressed as

$$n_e = B^2 Z \frac{I_e m_n v_n}{m_e < s\,v > \dot{m}_n V_d} \qquad (4)$$

All of the operating and geometric parameters except *D* are contained in Eq. (4).

Figure 7 shows the relation between the oscillation amplitude and n_e assuming that neutral temperature is 1,000[K] and electron temperature is 10[eV]. I_d is taken as I_e.

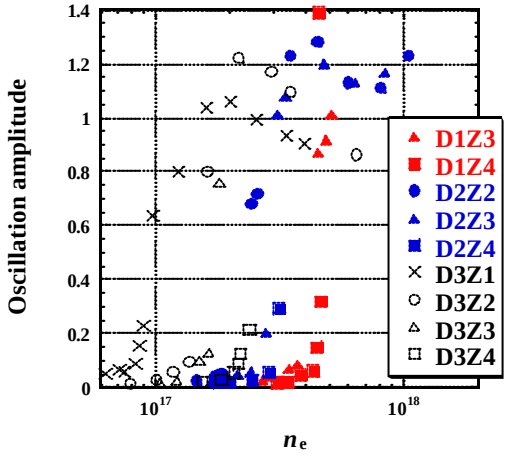

Fig. 7 Relation between n_e and oscillation amplitude. *Z*=1-4[mm], *D*=1-3[mm], *B*=0.006-0.02 [T]

In order to have clear insight from these data, we have to assume additional acceleration zone length Z_0 depending on *D* as

$$n_e = B^2 (Z + Z_0) \frac{I_e m_n v_n}{m_e < s v > \dot{m}_n V_d} \qquad (5)$$

As illustrated in Fig. 8, Z_0 would be increased with D because of penetrations of the plasma acceleration zone into the hollow. Z_0 was deduced by fitting a curve to a set of data for each D. They are listed in Table 2.

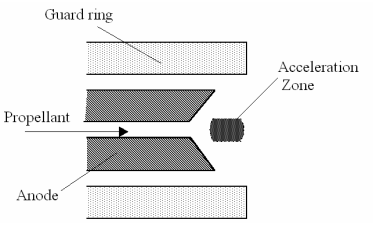

(a) D=1[mm].

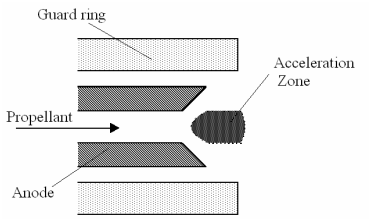

(b) D=2[mm].

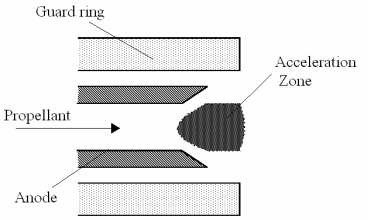

(c) D=3[mm].

Fig. 8 Substantial acceleration zone.

Table 2 The fitted value of Z_0.

	Z_0[mm]
D=1[mm]	0
D=2[mm]	2
D=3[mm]	4

The rearranged plots using n_e expressed in Eq. (5) is shown in Fig. 9. Oscillation amplitude was increased sharply at critical n_e of about 5×10^{17}[m^{-3}].

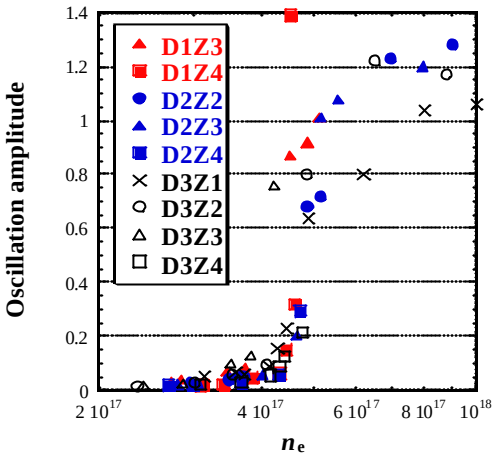

Fig. 9 Relation between n_e and oscillation amplitude taking into account of the substantial acceleration zone. Z=1-4[mm], D=1-3[mm], B= 0.006-0.02[T]

In the region where discharge is oscillating, electron diffusion coefficient would be no more classical, but anomalous. Therefore, actual electron density will be smaller than predicted one in that region.

CALCULATION

Computational Methods and Physical Models

It is very difficult to measure the distributions of electric potential and plasma density inside a hollow anode, structure of electrical sheath structure inside the hollow anode was numerically computed using fully kinetic 2D3V Particle-in-Cell (PIC) and Direct Simulation Monte Carlo (DSMC) methodologies. Figure 10 shows the flow chart of calculation.

One thousand of real particles are treated as one macro particle and both of electron and ion macro particles are treated kinetically. Electric and magnetic forces are implemented via the PIC method and collisions are via the DSMC method. The cylindrical coordinate system (r, z, q) was applied to the region inside the hollow anode as shown in Fig. 11. Particle's position is expressed in two-dimensional space r and z, while its velocity is expressed in three-dimensional space. That is, particles move in all directions, but the azimuthal coordinate is always discarded.

An orthogonal calculation grid is set, with the axial length of the cell getting smaller toward the anode exit in order to observe the sharp fall of electron density in the vicinity of anode exit. The minimum cell length is in the same order of the Debye length.

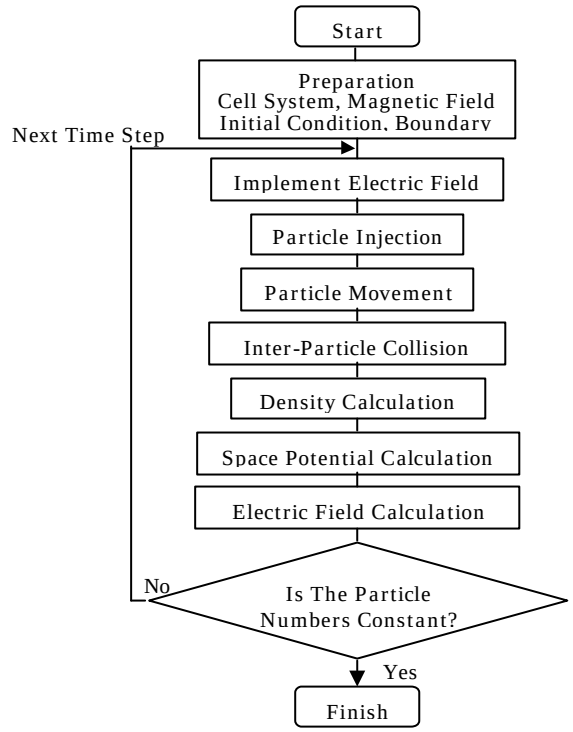

Fig. 10 Flow chart of the calculation.

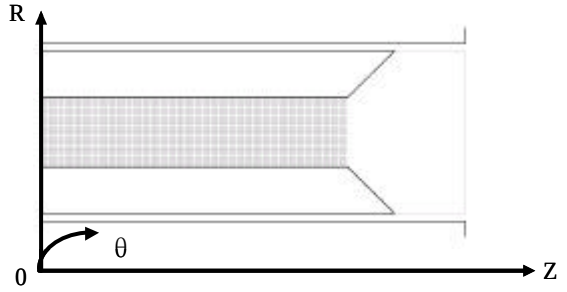

Fig. 11 The coordinate and the calculation grid.

Assumptions are listed below.

- Magnetic field lines are aligned in the radial direction uniformly inside the hollow anode and don't have axial or azimuthal components. B=0.01[T].
- Only singly charged ionization is considered.
- Mass ratio m_i/m_e is decreased from 4×10^{-6} to 1/100, to speed up heavy particle's motion.
- Potential difference between anode and plasma at the anode exit boundary is set 50 V.

Electrons are fed from the anode exit with a T_e=10[eV] half-Maxwellian velocity distribution. The electron density on that boundary n_{e0} is a variable parameter in this calculation.

Collisions considered in this simulation are shown in Table 3. The mean free time and collision frequency in the table are typical values when the particles are at their thermal velocity. The simulation time step is based on electron - neutral collision mean free time t_{en}.

Table 3 Collisions considered in the simulation.

Collision	Mean Free Time	Relative Collision Frequency
Electron–Neutral Elastic Scattering	2.038×10^{-9}[s]	1.00
Electron–Neutral Ionization	1.831×10^{-8}[s]	0.111
Electron–Neutral Excitation	6.683×10^{-8}[s]	3.05×10^{-2}
Electron–Ion Coulomb	2.827×10^{-7}[s]	7.21×10^{-3}
Electron–Electron Coulomb	1.527×10-5[s]	1.33×10-4
Neutral–Neutral Scattering	3.83×10-5 [s]	5.32×10-5

All the particles move according to the dynamic equations. The dynamic equations for charged particles are expressed as,

$$\text{Electrons:}\begin{cases} m_e\dfrac{dv_Z}{dt} = -e(E_Z - v_q B_R) \\ m_e\dfrac{dv_R}{dt} = -eE_r + m_e\dfrac{v_q^2}{x_R} \\ m_e\dfrac{dv_q}{dt} = -ev_Z B_R - m_e\dfrac{v_R v_q}{x_R} \\ \dfrac{dx_Z}{dt} = v_z, \quad \dfrac{dx_R}{dt} = v_R \end{cases} \tag{6}$$

$$\text{Ions:}\begin{cases} m_i\dfrac{dv_Z}{dt} = eE_Z \\ m_i\dfrac{dv_R}{dt} = eE_R \\ \dfrac{dx_Z}{dt} = v_Z \\ \dfrac{dx_R}{dt} = v_R \end{cases} \tag{7}$$

Space potential is calculated using the Poisson's equation as,

$$\frac{\partial^2 j}{\partial Z^2} + \frac{1}{x_R}\frac{\partial}{\partial R}\left(x_R\frac{\partial j}{\partial R}\right) = -\frac{e}{e_0}(n_i - n_e) \tag{8}$$

Results and Discussions

Computed distributions of electron and ion number densities, electric potential are shown in Fig. 12. In the region near the hollow exit, quasi-neutral plasma is created. As a result, electric sheath is retarded and the surface area of the sheath is enlarged in the hollow anode.

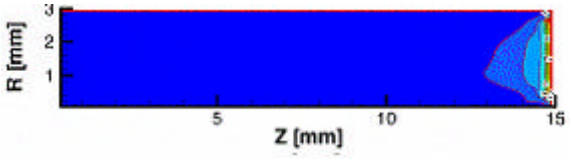

(a) Electron number density

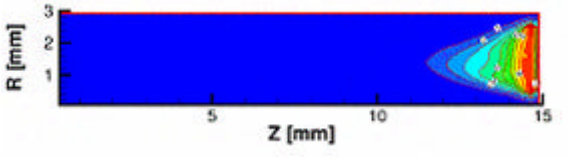

(b) Ion number density.

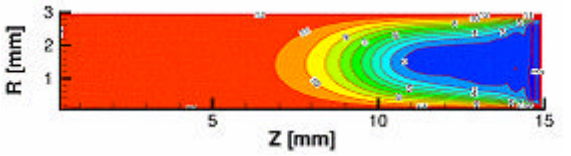

(c) Electric potential.

Fig. 12. Computed distributions of electron and ion number densities, electric potential

Figure 13 shows potential distributions for the cases D=1,3,6[mm]. The depth of quasi-neutral plasma region was increased with D, while it was not so sensitive to D.

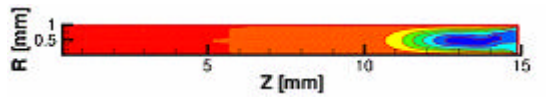

(a) D=1[mm].

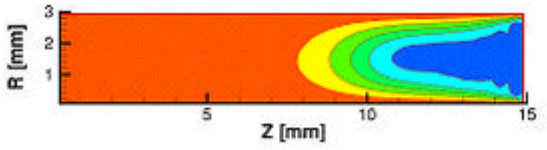

(b) D=3[mm].

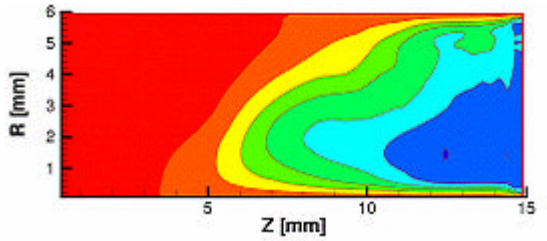

(c) D=6[mm].

Fig. 13 Electric potential distribution in the case of $n_{e0}=1 \times 10^{17}[1/m^3]$.

The correlation between plasma density on the anode exit boundary and sheath structure inside the hollow anode is our next concern.

CONCLUSIONS

In the experiment, it was found that there was a plasma density threshold for stable discharge. The computed sheath structure inside a hollow anode showed that electric sheath is distorted because of the existence of quasi-neutral plasma near the hollow exit. The depth of quasi-neutral plasma region in the hollow was not so sensitive to the hollow width.

REFERENCES

[1] Choueiri, E. Y., "Fundamental difference between the two Hall thruster variants", Physics of Plasmas Vol.8, No.11 November 2001.

[2] Semenkin A.V., Tverdokhlebov S.O., Garkusha V.I., Kochergin A.V., Chislov G.O., Shumkin B.V., Solodukhin A.V., Zakharenkov L.E., "Operating Envelopes of Thrusters with Anode Layer", IEPC2001-013, 27th International Electric Propulsion Conference, Pasadena, USA, October 2001.

[3] Semenkin, A., Kochergin, A., Garkusha, V., Chislov, G., Rusakov, A., "RHETT/EPDM Flight Anode Layer Thruster Development", IEPC-97-106, 25th International Electric Propulsion Conference, Cleveland, USA, August 1997.

[4] Yamamoto, N., Nakagawa, T., Komurasaki, K., Arakawa, Y., "Extending Stable Operation Range in Hall Thrusters", AIAA-2002-3953 38th AIAA/ASME/SAE/ASEE Joint Propulsion Conference & Exhibit, Indianapolis, USA, July 2002.

[5] Hirakawa, M., "Particle Simulation of Plasma Phenomena in Hall Thrusters", IEPC-95-164, 24th International Electric Propulsion Conference, Moscow, Russia, September 1995.

[6] Szabo, J. J., "Fully Kinetic Hall Thruster Modeling", IEPC-01-341, 27th International Electric Propulsion Conference, Pasadena, USA, October 2001.

[7] Szabo, J. J., "Fully Kinetic Hall Thruster Modeling of a Plasma Thruster", PhD Thesis, Massachusetts Institute of Technology, 2001.

[8] Szabo, J., Rostler, P., "One and Two Dimensional Modeling of the BHT-1000", IEPC-02-231, 28th International Electric Propulsion Conference, Toulouse, France, March 2003.